



Axial restraint forces in shear endplates of steel frames due to fire



Elie G. Hantouche*, Sarah A. Sleiman

Department of Civil and Environmental Engineering, American University of Beirut, Lebanon

ARTICLE INFO

Article history:

Received 4 January 2016
Received in revised form 21 September 2016
Accepted 30 September 2016
Available online 4 October 2016

Keywords:

Shear endplate
Fire
Finite element
Steel
Mechanistic
Axial restraint force

ABSTRACT

The results of a series of finite element (FE) simulations and experimental studies are used to develop a mechanistic model that predicts the axial restraint forces in steel shear endplate beam–column connections during a fire. First, FE models are developed to predict the total force–rotation response and failure modes, and are validated against experimental results available in the literature at both ambient and elevated temperature. Second, a parametric study is conducted to investigate some major parameters that impact the behavior of shear endplate connection assemblies during a fire. This includes beam length, load ratio, fire intensity, and endplate thickness. Based on FE and experimental results, a mechanistic model is proposed for the connection of typical steel frames subjected to fire exposure. The characteristics of the proposed model such as stiffness, tension and compression forces are determined based on each component of the connection. The proposed model is capable of predicting the axial restraint forces in shear endplate connections of typical steel frames for different geometric properties, under varied loading conditions, and elevated temperatures. The results can help inform future design guidelines to account for the thermal induced forces in shear endplate connections during a fire.

© 2016 Elsevier Ltd. All rights reserved.

1. Introduction

Shear endplate connections, also known as flexible endplates are widely used to connect steel beams to columns or girders in multi-story buildings. These connections possess large rotational ductility, and are considered as pinned joints. According to the design guidelines at ambient temperature, only gravity loads are accounted for in the procedure. However, during a fire event, shear or pinned connections are subjected to large axial forces, rotational demands, and significant loss of strength and stiffness [1]. Bailey et al. [2] stated that the axial restraint provided against the thermal expansion of beams results in compressive forces in the heating phase of the fire. At the end of the heating phase, tensile forces start to develop. Furthermore, tension develops in the connections as the beams contract during the cooling phase of the fire. The large thermally induced forces may result in failure of the connections during or after fire.

Many experimental and analytical studies were conducted in the past few years to understand the behavior of shear endplate connections at elevated temperature. Al-Jabri [3,4] and Al-Jabri et al. [5,6] conducted an experimental investigation to study the performance of composite shear endplate connections in fire. Also, a mechanistic model was developed by the same authors to predict the moment–rotation of the connections at elevated temperature. However, these studies and models only apply for the case of unobstructed rotation about the lower edge of the

endplate, assuming no contact between the beam and column flange. Also, no prediction of the thermally induced forced on the connection was reported. In addition, Hu et al. [7,8] investigated the capacity strength of shear endplate connection in fire both experimentally and analytically. The governing failure mode encountered was plate rupture in the vicinity of the weld. Yu et al. [9] developed a mechanistic model for simulating the behavior of isolated flexible endplates in fire.

Studies were also conducted on other types of shear connections such as shear tab, double angle, top and seat angle, and extended endplate connections. For instance, Wang et al. [10,11] developed a mechanistic model to predict the temperature–rotation of extended endplate bare-steel joints at elevated temperature. Hu and Engelhardt [8,12] conducted experiments and FE simulations to study the behavior of shear tab connections at elevated temperature, and to characterize their stiffness, strength, deformation capacity, and failure modes. They also studied the impact of several parameters on the connection response. In addition, Daryan and Yahyai [13] conducted experimental tests and FE simulations to study the behavior of bolted top and seat angle connections in fire. Kodur et al. [14] developed FE models to predict the behavior of typical beam–slab assemblies with different shear connection types exposed to different fire scenarios. In a very recent work, Selamet and Garlock [15,16,17] studied the behavior of shear tab, single angle, and double angle shear connections in fire. The connections were tested as part of a subassembly. They showed that the different shear connection types have similar global behavior. The response was governed by beam local buckling near the connection. Despite the progress that was made in understanding the capacity of shear endplate connections at elevated temperature, limited research has

* Corresponding author at: Department of Civil and Environmental Engineering, American University of Beirut, P.O. Box 11-0236, Riad El-Solh, Beirut 1107 2020, Lebanon.
E-mail address: eh12@aub.edu.lb (E.G. Hantouche).

been conducted to predict the thermal induced forces encountered in shear endplates during a fire event. Existing work available in the literature did not include possible parameters (such as beam length, load ratio, endplate thickness, and fire intensity) that affect connection failure in fire (Al-Jabri [3,4], Al-Jabri et al. [5,6], Hu et al. [7,8], and Yu et al. [9]). Also, the component-based models available in the literature considered only isolated connections and did not include the prediction of the axial restraint forces in shear endplate connections of typical steel frames at elevated temperatures. Conducting an extensive experimental investigation is time consuming and not economically feasible since it requires large scale heating facilities. FE analysis can be used as an alternative after a thorough validation with existing experimental results of isolated shear endplate connections at elevated temperature.

It should be noted that the main focus of this paper is to predict the fire induced axial restraint force in shear endplate connections of typical steel frames due to fire exposure. First, FE models of isolated shear endplate connections at ambient and elevated temperatures are developed to predict total force-rotation response and failure modes, and validated against experimental results available in the literature. Second, FE models of the connection assembly are generated and used to conduct an extensive parametric study to identify the key parameters that affect the behavior of the connection. The results of the study are then used to develop a mechanistic model that predicts the thermal induced axial forces during a fire.

2. Isolated shear endplate connection

The FE model of the shear endplate connection is developed. The aim is to determine the force rotational response of the connection at elevated temperature and to predict the capacity and failure mode, assuming no induced thermal forces. The FE results of shear endplate connections are compared with those obtained in the experimental program at University of Sheffield [18].

2.1. Development of the FE model

The FE model of the shear endplate connection is developed to reproduce the experimental results conducted at the University of Sheffield [18]. An overall view of the model is shown in Fig. 1(a). The FE model of the connection is developed in ABAQUS [19].

2.2. Geometry of the connection components

The shear endplate connection used in the analysis consists of a PL $8 \times 6 \times 0.4$ in. (PL $200 \times 150 \times 10$ mm) bolted to the flange of a W10 \times 60 (UC 254×89) column and welded to the web of a W12 \times 26 (UB 305×40) beam cross-section. Details of the connection configuration can be found in [18].

2.2.1. Geometric and force boundary conditions

The model is loaded in two steps. In the first step, a pretension force is applied to the bolts. The bolt pre-tensioning is modeled by applying a body force in the bolts equivalent to the minimum required pretension force specified in the AISC specifications [20]. In the second step, an inclined force is applied at the tip of the beam (Fig. 1(a)), to produce combined shear and tension forces. The initial loading angle is 35° for the cases where the temperature is 20°C , 450°C , and 550°C , and 45° for the case where the temperature is 650°C . Throughout the load step, the loading angle varies and is described in the experimental program [18]. Boundary conditions are applied on the system throughout the analysis as shown in Fig. 1(a).

2.2.2. Material properties

An idealized bilinear model is used for the steel materials. The ambient temperature mechanical properties used for the beam are: the yield stress $F_y = 52$ ksi (356 MPa), and the ultimate stress $F_u = 73$ ksi (502 MPa)

which are in accordance with Hu et al. [7]. For the shear endplate, the material model specified in Hu et al. [7] with $F_y = 50$ ksi (350 MPa) and $F_u = 66$ ksi (455 MPa) is incorporated in the FE model. For the column, the ambient-temperature mechanical properties used are A572Gr50 (S355) as specified by the experimental program [18]. For the structural bolts, an elastic-perfectly plastic material model is used. The ambient-temperature mechanical properties incorporated in the FE model for the structural bolts are: $F_u = 135$ ksi (930 MPa) which are in accordance with Hu et al. [7]. At elevated temperature, retention factors proposed by Lee et al. [21] are used for the base material whereas the retention factors proposed by the AISC specifications [22] and Eurocode 3 [23] are used for the bolts and welds, respectively. The retention factors for mechanical properties of structural bolt, weld, and steel materials incorporated in connection simulations can be found in Fig. 1(b).

2.2.3. Model discretization

All the connection components are meshed with eight-node brick elements with reduced integration (C3D8-R). Fig. 1(a) shows the mesh configuration of the model. To improve the accuracy of predictions, a finer mesh is used around the connection region, where failure is likely to occur. A mapped meshing technique is used to discretize bolts and their surrounding areas to account for stress concentration around the bolt-holes. The contact between the bolts and base material is modeled using surface to surface interaction with finite sliding. Finite sliding allows separation, sliding, and rotation of contact surfaces. A friction coefficient of 0.25 is utilized to model friction between the contact surfaces. The fillet welds are tied to adjacent parts by means of tie constraints applied at the contact surfaces.

2.2.4. Analysis procedure

To predict the strength of the flexible endplate connection at elevated temperature, steady state analysis is conducted. After heating the structure up to the desired temperature (20°C , 450°C , 550°C , and 650°C), a concentrated inclined load is applied while keeping the temperature constant, until failure of the connection. Note that the post ultimate behavior of the structure is not predicted. The objective is to identify the limit states in the connection at the specified temperatures under combined tension and shear loads.

2.2.5. FE vs. experimental predictions

The FE results are plotted against the experimental test results conducted at the University of Sheffield [18]. FE results show good agreement when compared to experimental results, as far as strength, stiffness, and rotation (Fig. 2).

The deformed shape and the failure mode of the shear endplate connection at ambient and elevated temperature are shown in Fig. 3(a), (b), (c), and (d). It can be seen from Figs. 2 and 3 that the FE simulation can predict closely the total force-rotation response of the connection as well as the failure mode which is plate rupture at the toe of the weld. Note that yielding is assumed to be the failure criteria.

The results of the capacity predictions and the comparison between the experimental and FE results are summarized in Table 1. The FE models predict the peak connection strength well.

3. Shear endplate connection assembly: evaluations of demand

Shear endplate connections are generally designed to resist gravity loads only. However, in fire, large axial forces can develop in the beam-end connection. To investigate the connection behavior in such conditions, a series of studies is conducted using 3D FE models in ABAQUS. The overall goal is to gain further insight into major key parameters that impact the performance of beam-to-column shear endplate connections in a fire.

In the FE model, several limitations are considered. The analysis is unable to predict the connection performance after first component fracture; the concrete floor system is not included in the models. Also

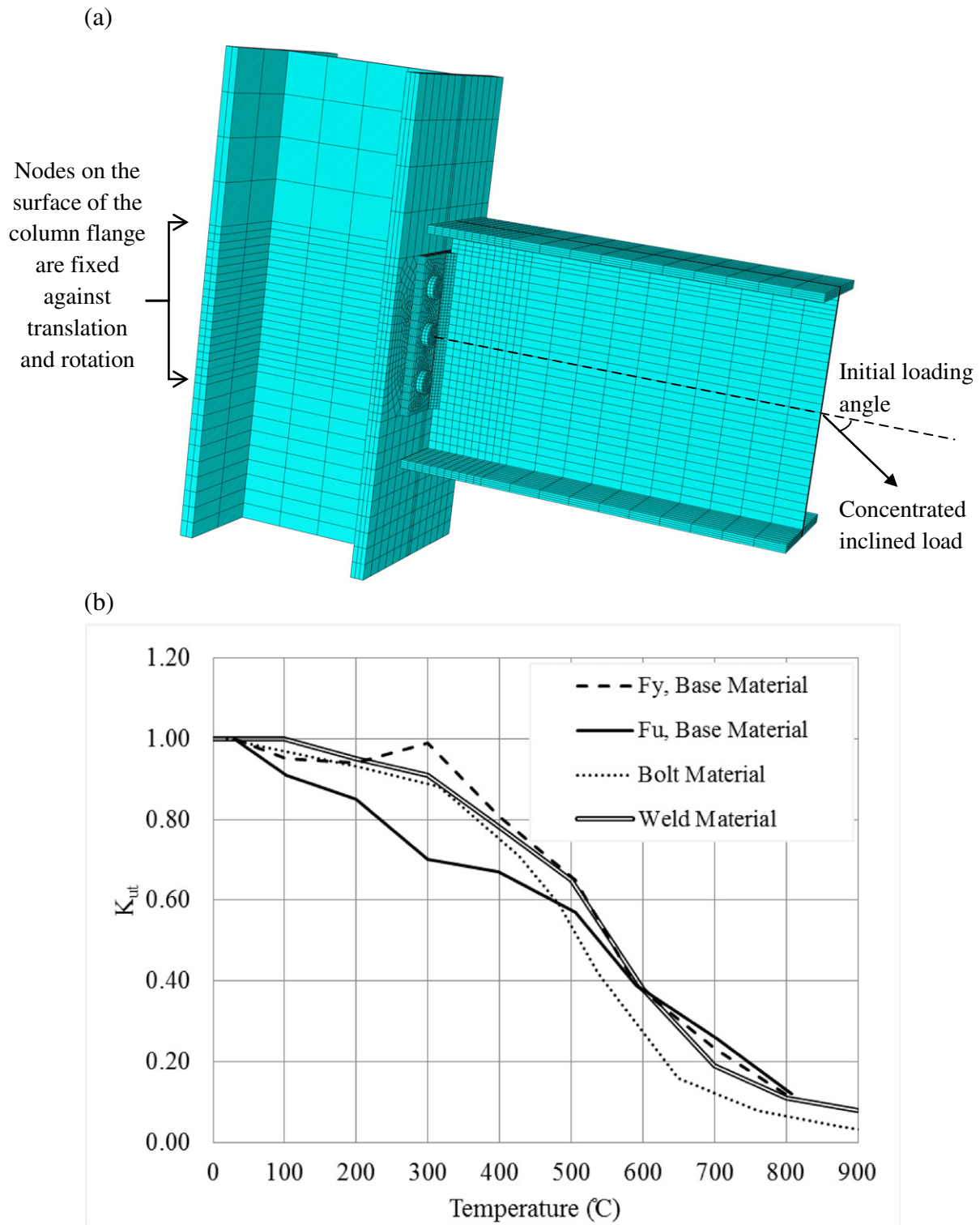


Fig. 1. (a) Connection details in FE model, (b) Strength retention factors for structural steel, structural bolts, and weld material at elevated temperatures.

the “*P-delta effect*” and thermal gradient are not accounted for in the analysis.

A series of FE models of typical floor beams with shear endplate connections are developed and analyzed. Parametric study is performed to examine the effects of several loading variables and boundary conditions on the behavior of shear endplate connections in fire. Also, a number of connection details that may affect the connection performance are investigated.

3.1. Description of the connection assembly model

A $W16 \times 36$ floor beam spanning between $W14 \times 90$ columns is used in the parametric study. Beams having 20 ft. (6.10 m), 30 ft. (9.15 m), and 40 ft. (12.20 m) length are selected for analysis. The beam ends are attached to the columns using shear endplate connections welded to the beam web and bolted to the column flange, as shown in Fig. 4. The ambient temperature material properties for the

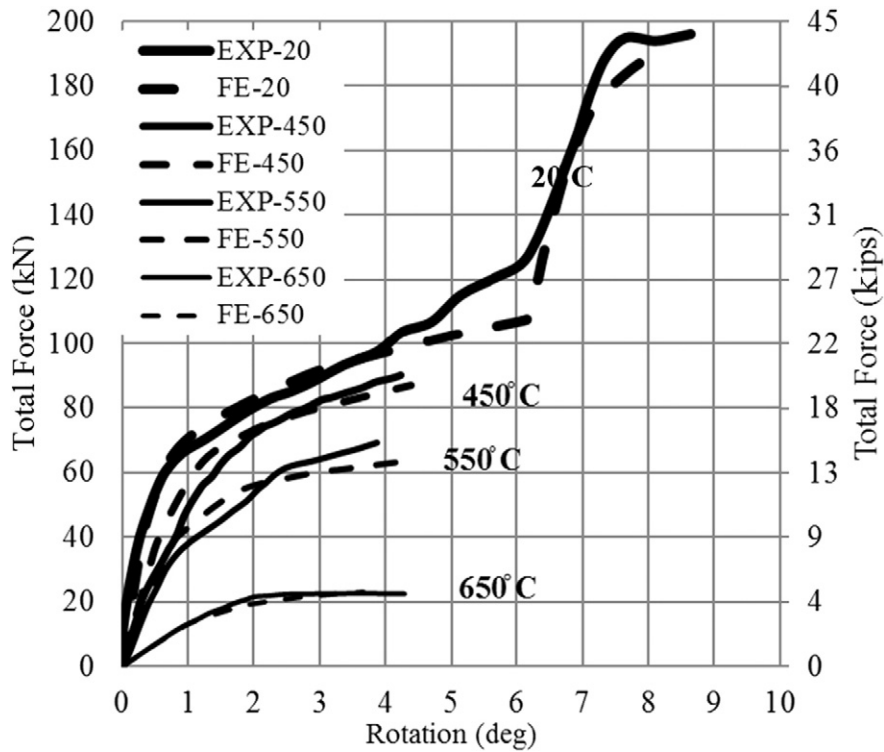


Fig. 2. Force-rotation behavior of shear endplate connections at ambient and elevated temperature: FE vs. experimental results.

structural bolts and steel materials that are used in the FE simulations are similar to the ones used by Hu and Engelhardt [8] in a previous study on shear tab connections. The column segments used in the model are 10 ft. (3.05 m) long and assumed pinned at both the top and bottom ends. The beam is modeled as simply supported, and thus the maximum moment developed at mid-span is equal to $wl^2/8$, where w is the applied load and l is the span length. The shear endplate connection corresponding to W16 × 36 beam is designed for a gravity load that produces a moment equal to the plastic moment of the beam. ASTM A490 bolts are used in the model and the retention factors proposed by Eurocode3 [23] are used to define the elevated temperature material properties of these bolts. The retention factors proposed by Lee et al. [21] are used to define the material properties of the base material at elevated temperature. A uniformly distributed load is applied to the beam. The magnitude of the distributed load is chosen to produce a maximum moment equal to a certain ratio of the plastic moment capacity of the beam at ambient temperature. Transient analysis is performed, which means that the applied load is held constant on the beam while temperature is changing. The beam and the shear endplate are heated as shown in Fig. 4. The remaining parts of the model are assumed to be insulated. The temperature is assumed to increase linearly with time and uniformly distributed in the heated parts of the structure. The temperature is increased to 650 °C and then cooled down to 20 °C.

3.2. Effect of key parameters and connection details

Several key parameters are studied including load ratio, beam length, fire intensity, and endplate thickness.

3.2.1. Load ratio

The load ratio is defined as the ratio of the maximum moment developed in the beam to the nominal plastic moment capacity of the beam section M_p . The length of the beam is 30 ft.

(9.15 m), which is a typical span length encountered in buildings. The load ratios used in the analysis are 0.25, 0.50, and 1.00.

Fig. 5 shows the variation of axial force with temperature. It can be seen that when the load ratio is 1.0 (full plastification of the beam section), the maximum compressive force on the connection is significantly reduced as compared to the cases where the ratio is 0.25 and 0.50. This is due to the fact that the beam has already yielded and cannot develop any additional thermal induced compressive forces. In addition, for the case when the load ratio is 1.0, yielding mechanism in the shear endplate occurs leading to an increase in the beam rotation early in the heating phase. Thus, tensile stresses develop in the bolts, and failure occurs at around 310 °C. When increasing the load ratio from 0.25 to 0.50, no significant variation of the connection axial force during either heating or cooling stages is observed, and the bolts fail at around 530 °C. Also, the analysis shows that a higher load ratio produces less compression force in the beam but higher tension force when catenary action develops.

In conclusion, increasing the load ratio limits the maximum axial compressive force in the beam. Nevertheless, it can cause early tension bolt failure and yielding of the endplate.

3.2.2. Beam length

A study on the effect of beam length on the connection behavior in fire is performed. Beams having 20 ft. (6.10 m), 30 ft. (9.15 m), and 40 ft. (12.20 m) length are selected for analysis. For all beams, the load ratio is chosen to be 1/3. Results are plotted in Fig. 6. The FE results show that although longer beams develop higher compressive force, the maximum axial compressive force on the connection for longer beams occurs at a lower temperature (Fig. 6). For the 40 ft. (12.20 m) beam, tension bolt failure occurs at about 490 °C while tension bolts in the other connections with beam length of 20 ft. (6.10 m) and 30 ft. (9.15 m) fail at 550 °C.

In conclusion, the beam length affects the behavior of the connection, where a longer beam develops a higher maximum axial compressive force and an earlier tension bolt failure.

3.2.3. Fire intensity

The fire intensity is defined as the highest temperature reached in a fire event. To study the effect of this parameter on the behavior of the

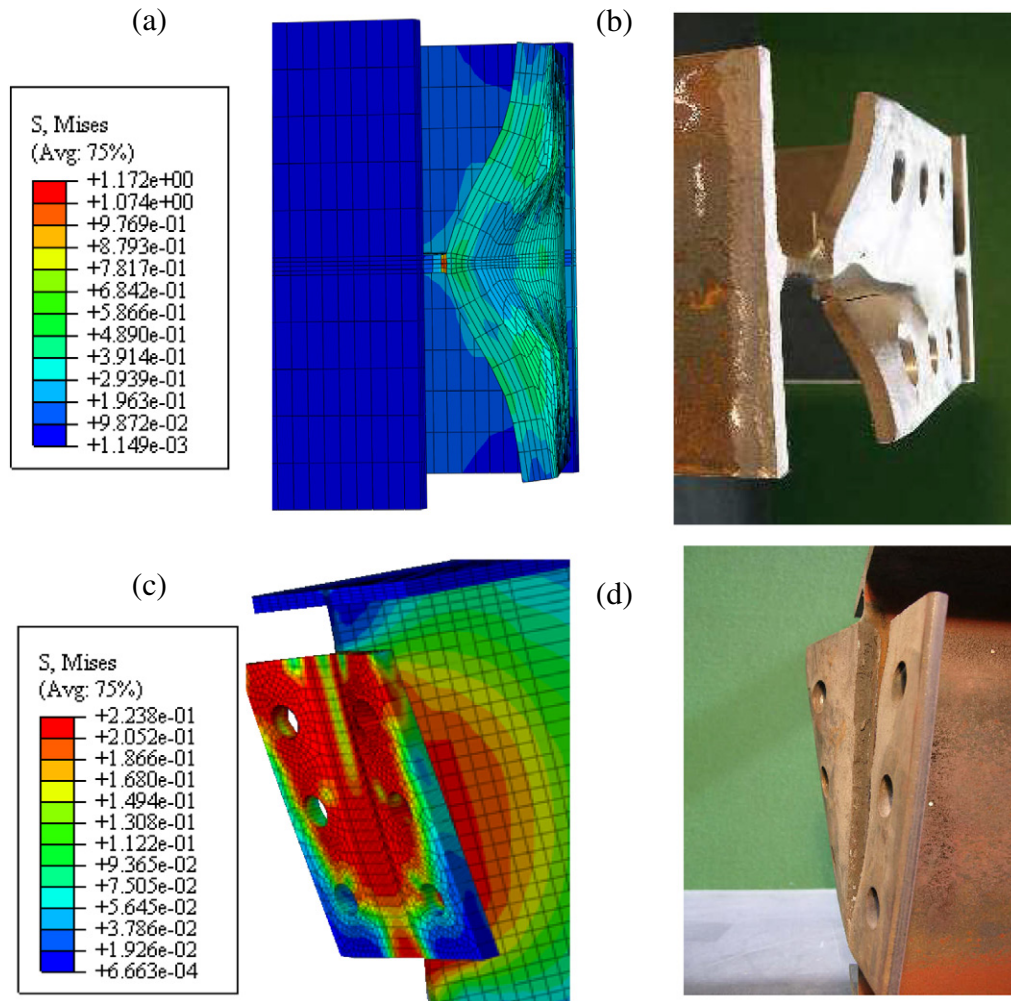


Fig. 3. (a) von Mises stress contours from FE simulation at 20 °C (plate rupture at toe of the weld), (b) Experiment results at 20 °C [18], (c) von Mises stress contours from FE simulation at 550 °C (plate rupture at toe of the weld), (d) Experiment results at 550 °C [18].

shear endplate connection, four 30 ft. (9.15 m) beams with a load ratio of 0.5 are used. The beams are heated up to 400 °C, 500 °C, 600 °C and 650 °C respectively, and then cooled back to 20 °C.

Fig. 7 shows the axial force in the connection versus temperature. It can be seen that higher fire intensity produces larger axial tensile force during cooling. Fig. 7 shows that for a fire intensity of 500 °C or less, no tension bolt failure occurs. This can be due to the additional loss of stiffness that occurs in the beam and connection as the temperature increases.

It can be concluded that for a fire intensity of 500 °C or less, no failure occurs, and the maximum compressive axial load is lower than for the case where the fire intensity is 600 °C or 650 °C.

Table 1
Shear endplate capacities: FE vs. experiment.

Temp (°C)	Exp. max load (kips)	FE max load (kips)	Failure mode ^a
Inclined tension			
20	43.16 (192 kN)	42 (185 kN)	Plate rupture
450	20.31 (90.36 kN)	19.3 (86 kN)	Plate rupture
550	15.4 (68.51 kN)	15 (66 kN)	Plate rupture
650	6.39 (28.45 kN)	5 (22 kN)	Plate rupture

^a The tabulated failure modes correspond to the ones observed in the experiments (initial loading angle is 35° for 20 °C, 450 °C, 550 °C, and the angle is 45° for 650 °C) which also were predicted in the FE models.

3.2.4. Shear endplate thickness

Another parameter included in this study is the plate thickness. To study the effect of this parameter on the connection behavior, two different thicknesses are considered: 0.375 in. (1 cm) and 0.5 in. (1.3 cm). The beam is 30 ft. (9.15 m) long with a load ratio of 0.5.

Fig. 8 shows the variation of the developed axial force in the connection for different endplate thicknesses. It can be seen that the maximum compressive force is greater for the 0.375 in. (1 cm) thick plate. Also, failure of tension bolts occurs at 500 °C and 550 °C for the 0.375 in. (1 cm) and the 0.5 in. (1.3 cm) thick plate, respectively. It can be concluded that decreasing the endplate thickness increases the plate uplift.

3.2.5. Shear endplate location

Another parameter considered in this study is the shear endplate location. The selected connection locations are: (1) at midheight of beam web, and (2) 1.25 in. (3.2 cm) above beam web. The results show no significant effect on the shear endplate connection behavior in fire. More detailed results are available in Hantouche and Sleiman [24].

4. Mechanistic modeling for predicting the thermal-induced axial forces of shear endplate connections in fire

Current U.S. building standards for structural fire resistance do not explicitly consider beam-to-column connections. During a fire, thermal induced axial forces develop in the beam and connection parts due to the

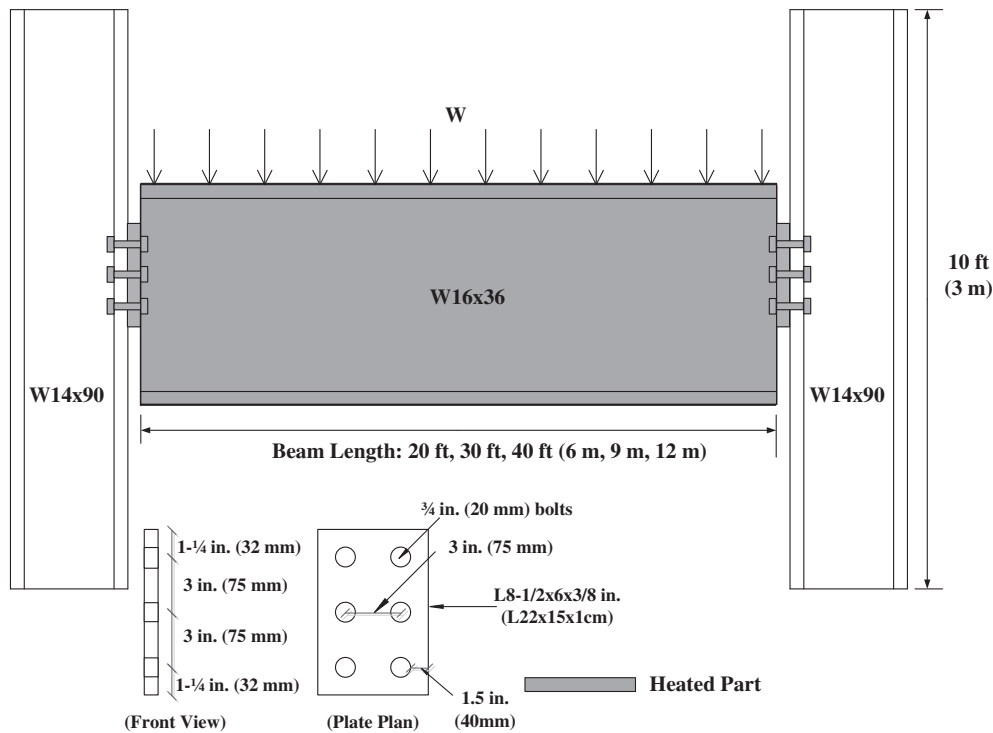


Fig. 4. Shear endplate connection assembly.

axial restraint provided by the connection. These axial forces are first compressive, and then become tensile when the structure loses stiffness and catenary action starts at a later stage of the heating during a fire.

The FE results show two types of mechanism of the beam-shear endplate connection (i) buckling of the beam web and lower flange subjected to a load ratio <0.85 (Type I), and (ii) yielding of the beam web and lower flange subjected to a load ratio >0.85 (Type II). Fig. 9(a) and (b) show a nonlinear behavior of the variation of the axial force with temperature in the beam-shear endplate connection for type I and type II mechanisms, respectively.

The parameters considered in the formulation of the proposed models are: beam length, endplate thickness, load ratio, column depth, column web thickness, and beam cross-sectional area. The proposed model allows design engineers to quantify the thermal induced forces and to predict the axial force versus temperature of beam-shear endplate connection during a fire event.

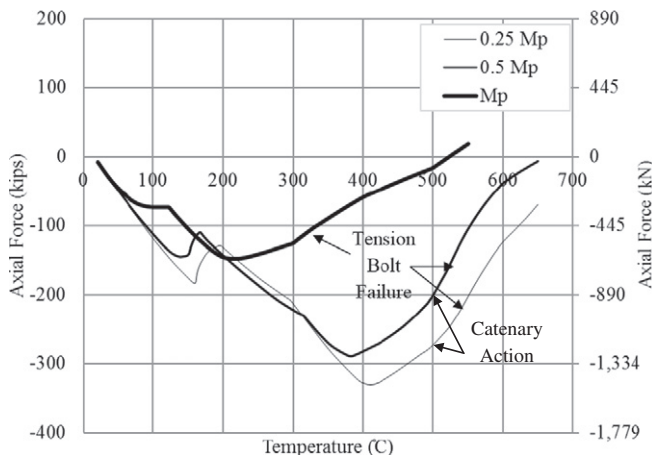


Fig. 5. Axial force in the shear endplate during heating and cooling for a varying load ratio.

4.1. Description of the behavior

4.1.1. Proposed model I

Fig. 9(a) describes the thermal induced axial forces in the beam at elevated temperature. The behavior is divided into four segments during the heating phase of the fire. As the temperature increases, the compressive axial force in the beam increases until the beam web buckles ($s1$). The axial load starts decreasing due to buckling of the beam web ($s2$). At the onset of contact of the beam flange and column flange, the axial force increases until it reaches a maximum value where beam flange buckling occurs ($s3$). At a certain temperature, an increase in beam deflection is accompanied by catenary action development in the beam ($s4$). The compressive axial force drops gradually and tension bolt failure occurs.

4.1.2. Proposed model II

Fig. 9(b) describes the thermal induced axial forces in the beam at elevated temperature. As the temperature increases, the compressive axial

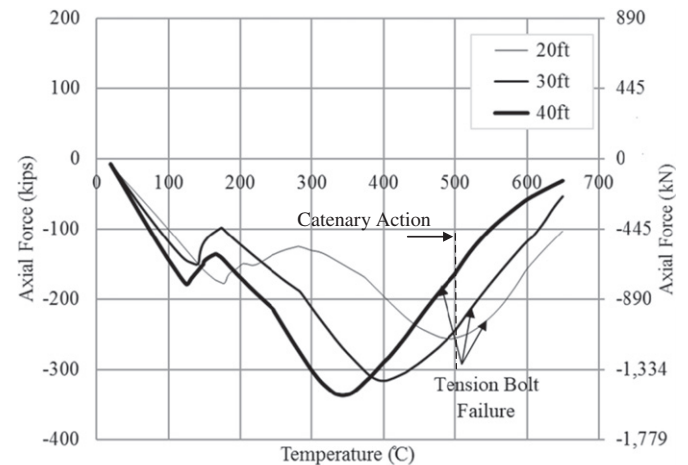


Fig. 6. Axial force in the shear endplate for varying beam lengths.

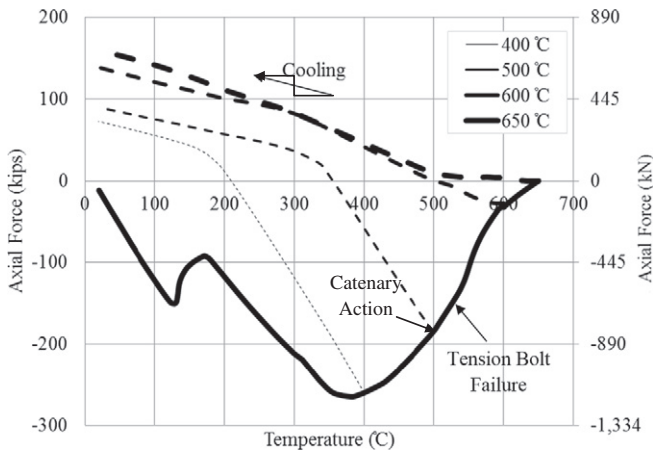


Fig. 7. Axial force in the shear endplate for varying fire intensities (solid lines are heating; dashed lines are cooling).

load in the beam increases until local web buckling occurs in the beam followed by beam web yielding (s1, s2, and s3). When contact occurs between beam flange and column flange, the axial force increases until it reaches a maximum value when local beam flange buckling occurs followed by beam flange yielding (s4 and s5). The yielding of the beam flange limits the compressive axial force. The compressive axial force drops gradually, and at a certain temperature, an increase in deflection leads to tension bolt failure (s6).

4.2. Elastic and plastic stiffness of the connection

The beam is modeled using a beam element and the connection and column parts are modeled using an equivalent axial spring.

Direct stiffness method is used to determine the thermally induced axial force in the beam and connection element.

The spring element stiffness matrix, $K_{s(i)}$ at temperature $T_{(i)}$, is given as:

$$K_{s(i)} = \begin{bmatrix} k_{(i)} & -k_{(i)} \\ -k_{(i)} & k_{(i)} \end{bmatrix}$$

where $k_{(i)}$ corresponds to the elastic or plastic stiffness of the spring element at temperature $T_{(i)}$, and can be computed according to Al-Jabri et

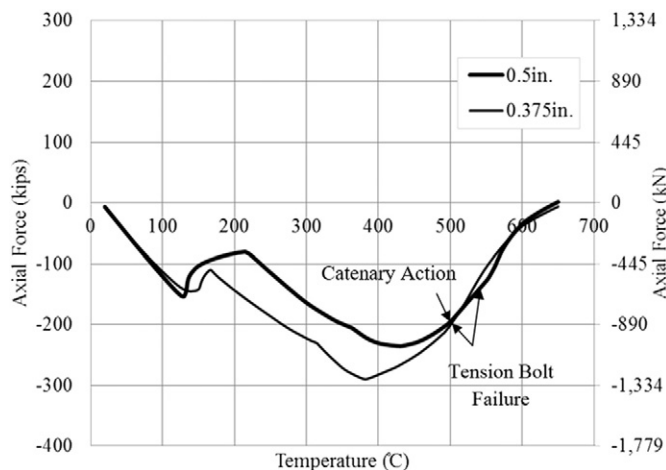


Fig. 8. Axial force in the shear endplate for a varying endplate thickness.

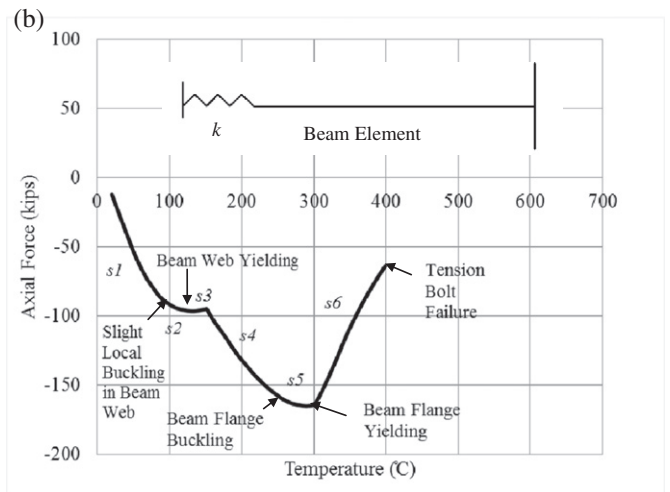
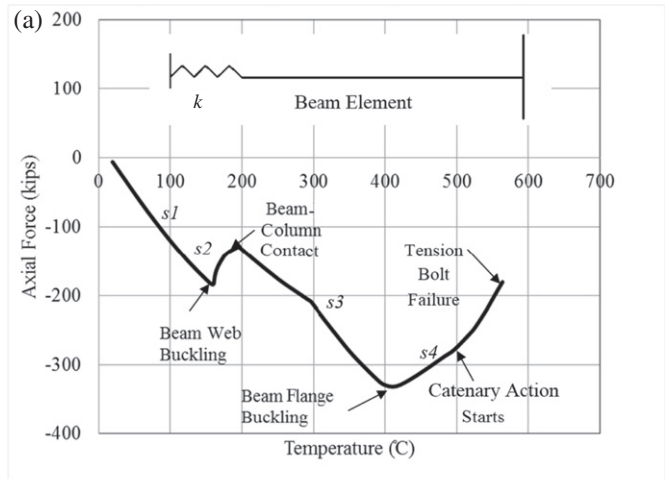


Fig. 9. Typical variation of the axial force with temperature for a shear endplate connection, (a) type I mechanism, (b) type II mechanism.

al. [6].

$$k_{(i)} = \begin{cases} \frac{E_{c(i)}t_{cw}b_{effcw}}{d_{cw}} & \text{for the elastic state} \\ \frac{E_{Tc(i)}t_{cw}b_{effcw}}{d_{cw}} & \text{for the plastic state} \end{cases} \quad (1)$$

where $E_{c(i)}$ is the modulus of elasticity of the column at temperature $T_{(i)}$, $E_{Tc(i)}$ is the tangent modulus of elasticity of the column at temperature $T_{(i)}$, t_{cw} is the thickness of the column web; b_{effcw} is the effective width of the column web (assumed equal to the depth of the endplate plus five times the distance from the outer face flange to the web toe fillet); and d_{cw} is the depth of the column web between fillets.

The stiffness equation becomes:

$$\begin{bmatrix} \frac{E_{b(i)}A_b}{L_b} & 0 & 0 & -\frac{E_{b(i)}A_b}{L_b} & 0 & 0 \\ 0 & \frac{12E_{b(i)}I_b}{L_b^3} & \frac{6E_{b(i)}I_b}{L_b^2} & 0 & -\frac{12E_{b(i)}I_b}{L_b^3} & \frac{6E_{b(i)}I_b}{L_b^2} \\ 0 & \frac{6E_{b(i)}I_b}{L_b^2} & \frac{4E_{b(i)}I_b}{L_b} & 0 & -\frac{6E_{b(i)}I_b}{L_b^2} & \frac{2E_{b(i)}I_b}{L_b} \\ -\frac{E_{b(i)}A_b}{L_b} & 0 & 0 & \frac{E_{b(i)}A_b}{L_b} + k_{(i)} & 0 & 0 \\ 0 & -\frac{12E_{b(i)}I_b}{L_b^3} & -\frac{6E_{b(i)}I_b}{L_b^2} & 0 & \frac{12E_{b(i)}I_b}{L_b^3} & -\frac{6E_{b(i)}I_b}{L_b^2} \\ 0 & \frac{6E_{b(i)}I_b}{L_b^2} & \frac{2E_{b(i)}I_b}{L_b} & 0 & -\frac{6E_{b(i)}I_b}{L_b^2} & \frac{4E_{b(i)}I_b}{L_b} \end{bmatrix} \Delta_{(i)} = P_{(i)} + FEF \quad (3)$$

(3)

where $E_{b(i)}$ is the modulus of elasticity of the beam at temperature $T_{(i)}$, I_b is the moment of inertia, L_b is the length of the beam, A_b is the cross sectional area of the beam, $\Delta_{(i)}$ is the vector of nodal displacements at temperature $T_{(i)}$, $P_{(i)}$ is the vector of external applied forces at the nodes at temperature $T_{(i)}$, and FEF corresponds to the *fixed end forces* (vector of forces induced by change in temperature).

The internal axial force in the beam, $P_{(i)}$, at temperature $T_{(i)}$, can be written as follows:

$$P_{(i)} = k_{(i)}\Delta = \frac{k_{(i)}E_{b(i)}A_b\alpha_{(i)}\Delta T}{\left(\frac{E_{b(i)}A_b}{L_b} + k_{(i)}\right)} \quad (3)$$

where $\alpha_{(i)}$ is defined as the coefficient of thermal expansion, and ΔT corresponds to the temperature increment.

4.3. Formulation of the response for proposed model I

4.3.1. Mechanism in (s1)

During the first stage of the heating phase of a fire (s1), the compressive axial force in the beam is mainly due to the endplate restraining the expansion of the beam web. The axial force at each temperature increment, ΔT , can be written as follows:

$$P_{(i)} = k_{(i)}\Delta = \frac{k_{(i)}E_{b(i)}A_{bw}\alpha_{(i)}(T_{(i)} - 20)}{\left(\frac{E_{b(i)}A_{bw}}{L_b} + k_{(i)}\right)} \quad (4)$$

where A_{bw} is the area of the beam web.

As the temperature increases, the axial force developed in the beam increases and two limit states might occur: either column web buckling, or elastic beam web buckling. The force that causes buckling in the column at elevated temperature, $P_{crbw(i)}$, and the effective buckling width of the column web, b_{eff-c} , can be written as follows, respectively [25]:

$$P_{crbw(i)} = 8.4b_{eff-c}^{0.017}d_c^{0.96}t_{cw}^{1.43}f_{ycw(i)}^{0.76} \quad (5)$$

$$b_{eff-c} = t_{bf} + 2\sqrt{2}a_p + 5(t_{cf} + r_c) \quad (6)$$

where d_c is the depth of the column, $f_{ycw(i)}$ is the column web yield strength at a given temperature, t_{bf} is the thickness of the beam flange, a_p is the size of the fillet weld, t_{cf} is the thickness of the column flange, and r_c is the root radius of the column.

A modified expression for computing the beam web critical buckling load is used based on Usmani et al. [26]. It is noted that $(A_{bw}/A_b)^2$ is added to account for the reduction of the moment of inertia of the beam at early stages of the fire (s1), since the beam web alone is contributing to the axial force in (s1).

$$P_{crbw(i)} = \frac{\pi^2 E_{b(i)} I_b}{L_b^2} \left(\frac{A_{bw}}{A_b}\right)^2 \quad (7)$$

At each temperature increment, the axial force $P_{(i)}$ is calculated and compared to $P_{crbw(i)}$ (Eq. (5)) and $P_{crbw(i)}$ (Eq. (7)). The incremental procedure continues until one of the two limit states is reached. Beam web buckling governs in all the cases studied.

4.3.2. Mechanism in (s2)

When local buckling of the beam web occurs, only part of the beam web area is considered in computing the axial force. To compute the axial force, the reduced beam web area, A_{bwr} , needs to be calculated.

First, the reduced beam web area is calculated at each temperature increment, ΔT :

1- The temperature at each increment is computed using the following equation:

$$T_{(i)} = T_{(i-1)} + \Delta T \quad (8)$$

where $T_{(i)}$ is the temperature at the current step, $T_{(i-1)}$ is the temperature at the previous step, and ΔT is the temperature increment.

2- The beam web area at any given temperature, $T_{(i)}$, can be written as follows:

$$A_{bwr(i)} = A_{bwr(i-1)} + \Delta A_{bwr} \quad (9)$$

where $A_{bwr(i)}$ is the beam web area at the current step, $A_{bwr(i-1)}$ is the beam web area at the previous step, and ΔA_{bwr} is the beam web area increment.

3- The axial load at any given temperature, $T_{(i)}$, is given as:

$$P_{(i)} = P_{(i-1)} + \Delta P \quad (10)$$

where $P_{(i)}$ is the axial force at the current step, $P_{(i-1)}$ is the axial force at the previous step, and ΔP is the axial force increment.

4- The beam web area at any given temperature, $A_{bwr(i)}$, can be written as a linear relationship:

$$\frac{A_{bwr(i)}}{A_{bw}} = a_1 \left(\frac{P_{(i-1)}}{P_{crbw}}\right) + b_1 \quad (11)$$

where P_{crbw} is the axial force at the end of (s1), a_1 and b_1 are constants, and their values can be found in Table 2. Note that a_1 and b_1 are dependent on the following parameters: beam web slenderness, load ratio, beam length, and endplate thickness, and the computation of a_1 and b_1 is presented below.

a_1 and b_1 are computed by conducting a parametric study that covers most possible cases associated with W16 × 36 beam. Load ratios of (0.25, 0.33, 0.5), endplate thicknesses of (0.375, 0.5, 0.6, 0.7 in.), and beam lengths of (20, 25, 30, 35, 40, 45 ft) are considered in computing a_1 and b_1 . Note that a constant beam web slenderness is considered in the study ($h/t_w = 48.1$, associated with W16 × 36 beam). It is found from the FE results that the axial compressive force decreases due to the reduced beam web area at each temperature increment. This is due to the post-buckling effect of the beam web.

The ratio of the reduced beam web area (from FE results) to the total beam web area, $(A_{bwr(i)}/A_{bw})$, is plotted against the ratio of the axial force (from FE results) to the critical beam web buckling load, $(P_{(i-1)}/P_{crbw})$ (Fig. 10(a)). The data points for each case are found to capture a linear fit with an acceptable coefficient of determination. The values of the slope (a_1) and y-intercept (b_1) for each case can be found in Table 2.

5- The axial force, $P_{(i)}$, at any given temperature, $T_{(i)}$, can be written as:

$$P_{(i)} = k_{(i)}\Delta = \frac{k_{(i)}E_{b(i)}A_{bwr(i)}\alpha_{(i)}(T_{(i)} - 20^\circ\text{C})}{\left(\frac{E_{b(i)}A_{bwr(i)}}{L_b} + k_{(i)}\right)} \quad (12)$$

The design engineer computes the critical buckling load, P_{crbw} , and the beam web area at the onset of buckling, A_{bw0} . Next, the values of

Table 2
Buckling and contact parameters for different load ratios, beam lengths, and endplate thickness.

Column section	Beam section	Case	Beam length ft. (m)	Endplate thickness in. (mm)	LR ^a	a ₁	b ₁	a ₂	b ₂
W14 × 90	W16 × 36	1	20 (6.1)	0.375 (9.53)	0.5	1.095	−0.266	0.323	−0.173
		2	20 (6.1)	0.375 (9.53)	0.33	1.256	−0.412	0.405	−0.230
		3	20 (6.1)	0.375 (9.53)	0.25	1.234	−0.385	0.455	−0.198
		4	20 (6.1)	0.5 (12.7)	0.5	1.278	−0.438	0.555	−0.221
		5	20 (6.1)	0.5 (12.7)	0.33	1.305	−0.459	0.740	−0.391
		6	20 (6.1)	0.5 (12.7)	0.25	1.122	−0.294	0.612	−0.222
		7	20 (6.1)	0.6 (15.24)	0.5	0.909	−0.152	0.496	−0.189
		8	20 (6.1)	0.6 (15.24)	0.33	1.092	−0.279	0.699	−0.236
		9	20 (6.1)	0.6 (15.24)	0.25	1.091	−0.277	0.795	−0.283
		10	20 (6.1)	0.7 (17.78)	0.5	1.141	−0.354	0.766	−0.275
		11	20 (6.1)	0.7 (17.78)	0.33	1.076	−0.280	0.709	−0.354
		12	20 (6.1)	0.7 (17.78)	0.25	1.077	−0.280	1.075	−0.635
		13	25 (7.62)	0.375 (9.53)	0.5	1.038	−0.118	0.492	−0.093
		14	30 (9.15)	0.375 (9.53)	0.5	2.946	−2.068	0.221	−0.067
		15	30 (9.15)	0.375 (9.53)	0.33	1.604	−0.768	0.330	−0.182
		16	30 (9.15)	0.375 (9.53)	0.25	0.917	−0.125	0.290	−0.186
		17	30 (9.15)	0.5 (12.7)	0.5	0.897	−0.147	0.352	−0.101
		18	30 (9.15)	0.5 (12.7)	0.33	2.432	−1.708	0.265	−0.217
		19	30 (9.15)	0.5 (12.7)	0.25	1.784	−0.937	0.418	−0.352
		20	30 (9.15)	0.6 (15.24)	0.5	1.071	−0.258	0.332	−0.092
		21	30 (9.15)	0.6 (15.24)	0.33	2.622	−1.805	0.378	−0.282
		22	30 (9.15)	0.6 (15.24)	0.25	1.783	−0.937	0.505	−0.290
		23	30 (9.15)	0.7 (17.78)	0.5	0.999	−0.227	0.343	−0.089
		24	30 (9.15)	0.7 (17.78)	0.33	1.132	−0.308	0.516	−0.213
		25	30 (9.15)	0.7 (17.78)	0.25	0.163	−0.836	0.511	−0.332
		26	35 (10.67)	0.375 (9.53)	0.5	1.226	−0.226	0.296	−0.105
		27	45 (13.72)	0.375 (9.53)	0.5	1.093	0.061	0.143	−0.072
		28	30 (9.15)	0.375 (9.53)	0.85	−0.41	1.364	1.913	−2.106
		29	30 (9.15)	0.375 (9.53)	0.9	−0.76	1.711	3.593	−4.135
		30	30 (9.15)	0.375 (9.53)	0.92	−0.43	1.408	1.524	−1.687
		31	30 (9.15)	0.375 (9.53)	1	−1.25	2.115	0.992	−0.241
		32	30 (9.15)	0.375 (9.53)	0.5	2.946	−2.068	0.221	−0.067

^a LR: load ratio.

a_1 and b_1 (Table 2) are used to calculate the reduced area at the first temperature increment in (s2), $A_{bwr(1)}$, with its corresponding axial force, $P_{(1)}$. The axial force, $P_{(1)}$, is used to calculate the reduced beam web area at the second temperature increment, $A_{bwr(2)}$. This incremental procedure continues until beam flange contact occurs. Contact is determined by checking the beam end rotation at each temperature increment. The beam end rotation at the onset of contact is equal to the geometric angle of contact between the bottom beam flange and the column, θ_c . It can be written as follows:

$$\theta_c = \frac{t_e}{l_1} \quad (13)$$

where t_e is the shear endplate thickness, and l_1 is the distance from the edge of the endplate to the external side of the lower flange of the beam.

The beam end rotation, $\theta_{(i)}$, for a simply supported beam in the elastic range, at any given temperature, $T_{(i)}$, is given by Selamet and Garlock [16]. A modification factor $p_{(i)}$ is added to the equation in order to reduce the moment of inertia of the beam, I_b , since part and not all the beam section is contributing to the force.

$$\theta_{(i)} = \frac{wL_b^3 p_{(i)}}{8E_{b(i)}I_b} \quad (14)$$

where w is the applied load on the beam, and $p_{(i)} = A_b/A_{bwr(i)}$.

4.3.3. Mechanism in (s3)

After contact, the lower beam flange is subjected to compression loading. The total axial load is now composed of two parts (contribution from beam web and beam flange) [16]. In this case, the total area of the beam section working in compression can be written as

follows:

$$A_{bc(i)} = A_{bwr} + A_{bfc(i)} \quad (15)$$

where $A_{bc(i)}$ is the total beam section area contributing to the axial force, A_{bwr} is the reduced beam web area at the end of (s2), and $A_{bfc(i)}$ is the contact flange area contributing to the axial force at each temperature increment. To compute the axial force, the flange contact area contributing to the axial force, $A_{bfc(i)}$, needs to be calculated.

First, the flange contact area is calculated at each temperature increment, ΔT , as follows:

- 1- The temperature at each increment, $T_{(i)}$, is computed using Eq. (8).
- 2- The flange contact area contributing to the axial force at any given temperature, $T_{(i)}$, can be written as follows:

$$A_{bfc(i)} = A_{bfc(i-1)} + \Delta A_{bfc} \quad (16)$$

where $A_{bfc(i)}$ is the flange contact area at the current step, $A_{bfc(i-1)}$ is the flange contact area at the previous step, and ΔA_{bfc} is the flange contact area increment.

- 3- The axial load at any given temperature is given by Eq. (10).
- 4- The flange contact area contributing to the axial force at any given temperature, $T_{(i)}$, can be expressed as a linear relationship:

$$\frac{A_{bfc(i)}}{A_{bf}} = a_2 \left(\frac{P_{(i-1)}}{P_{crbw}} \right) + b_2 \quad (17)$$

where a_2 and b_2 can be found in Table 2. Note that a_2 and b_2 are dependent on the following parameters: slenderness of the beam

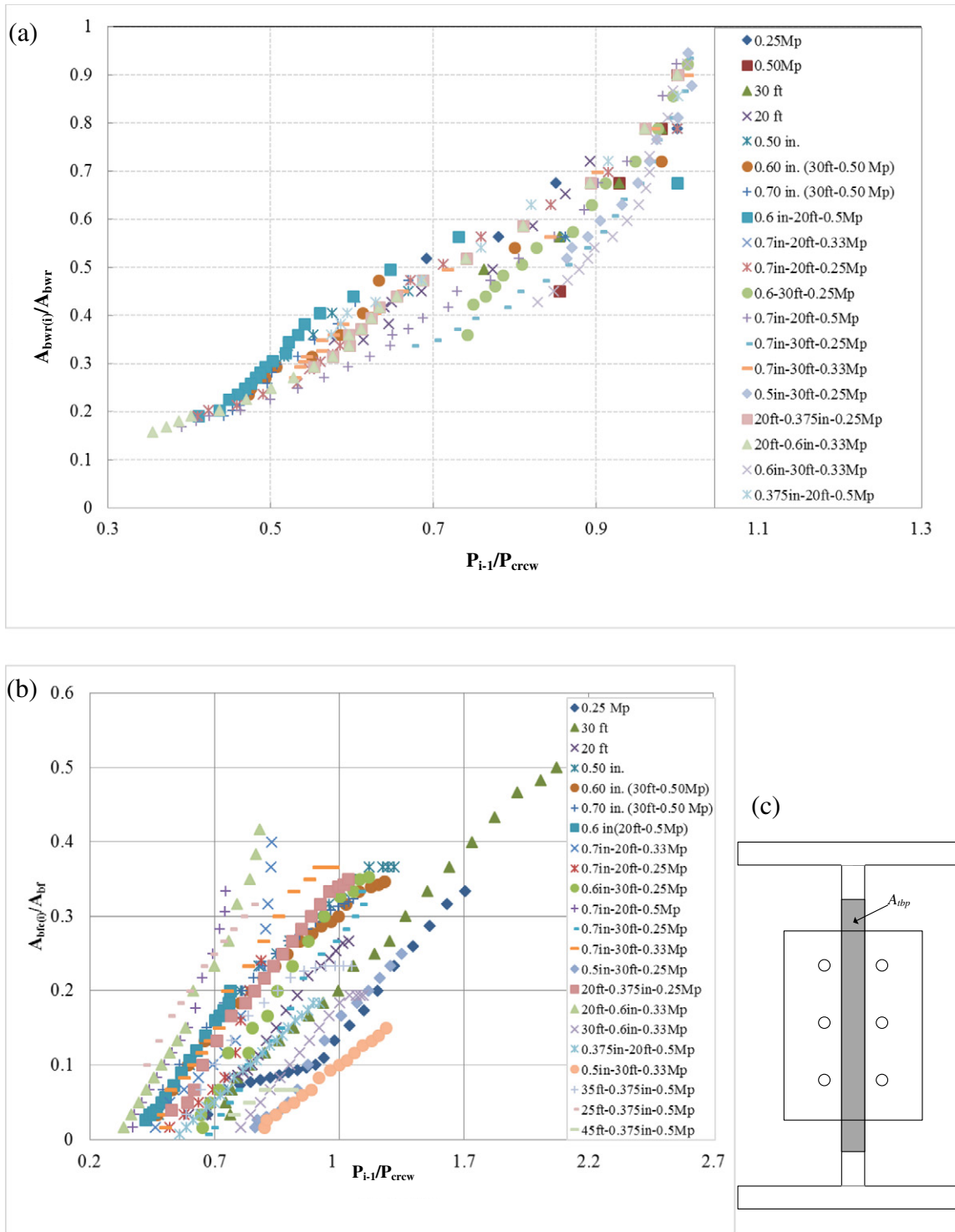


Fig. 10. (a) Reduction in the area of the beam web at the current step (i) as a function of the axial force at the previous step ($i-1$), (b) Increase in the flange contact area contributing to the axial as a function of the axial force at the previous step ($i-1$), (c) Tributary contact area of the beam web.

flange, load ratio, beam length, and endplate thickness, and the computation of a_2 and b_2 is similar to that of a_1 and b_1 and is presented below. a_2 and b_2 are computed from the same parametric study that is used to compute a_1 and b_1 (varying the load ratio, beam length and endplate thickness). Note that a constant beam flange slenderness is considered in the study ($b_f/2t_f = 8.12$, associated with W16 \times 36 beam). It is found from the FE results that the axial compressive force increases due to the lower beam flange contact area at each temperature increment.

The ratio of the flange contact area (from FE results) to the total area of the lower beam flange, $(A_{bfc(i)})/A_{bf}$, is plotted against the ratio of the axial force (from FE results) to the critical beam web buckling load, $(P_{(i-1)})/P_{crew}$ (Fig. 10(b)). The data for each case is found to capture a linear fit with an acceptable coefficient of determination. The values of the slope (a_2) and y-intercept (b_2) for each case can be found in Table 2.

5- The axial force, P_i , at any given temperature, T_i , can be written as follows:

$$P_{(i)} = k_{(i)} \Delta = \frac{k_{(i)} E_{b(i)} A_{bc(i)} \alpha_{(i)} (T_{(i)} - 20^\circ\text{C})}{\left(\frac{E_{b(i)} A_{bc(i)}}{L_b} + k_{(i)} \right)} \quad (18)$$

When the area of the beam flange increases, the total compressive axial force in the beam increases at each temperature increment. This increase is limited by plastic buckling of the lower flange of the beam at temperature T_{pmax} with a maximum axial force P_{max} and contact area $A_{bc(max)}$. A modified expression for computing the beam lower flange critical buckling load is used based on Usmani et al. [26]. It is noted that $(A_{fc(i)}/A_b)^2$ is added to reduce the moment of inertia of the

beam to that of the bottom beam flange.

$$P_{crbf(i)} = \frac{\pi^2 E_{b(i)} I_b}{L_b^2} \left(\frac{A_{fc(i)}}{A_b} \right)^2 \quad (19)$$

The contribution of the lower flange of the beam axial compressive force to the total force can be described as the difference between the total axial compressive force and the critical web buckling load:

$$P_{bfc(i)} = P_{(i)} - P_{crbw} \quad (20)$$

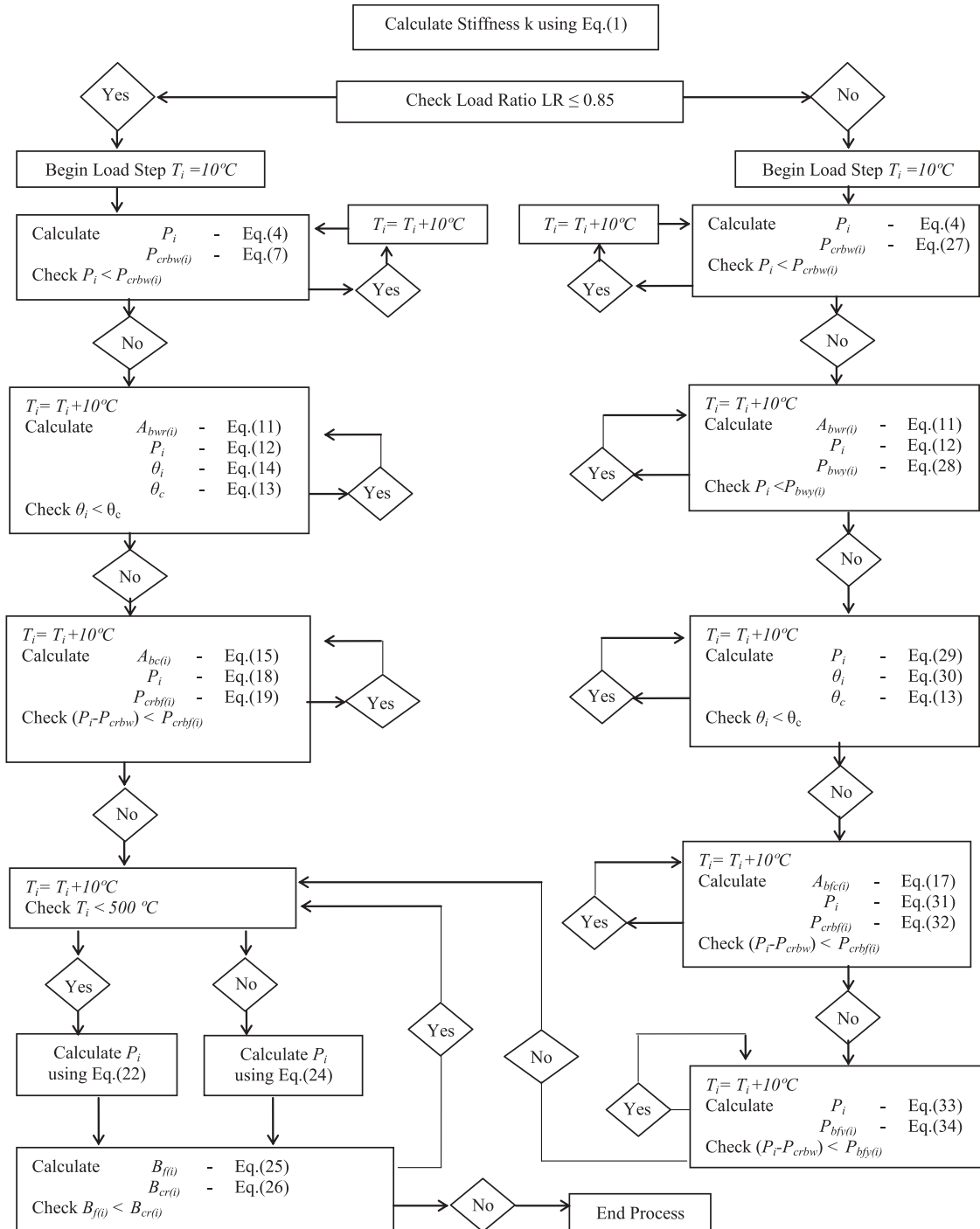


Fig. 11. Flowchart of the incremental stiffness shear endplate model.

Lower beam flange buckling occurs when the contribution from the lower beam flange, $P_{bfc(i)}$, reaches the critical lower flange buckling load, $P_{crbf(i)}$.

4.3.4. Mechanism in (s4)

After the onset of plastic lower flange buckling (s4), the beam contact area contributing to the axial force starts to plastify. It is observed from the FE results that the beam plastifies completely at 470 °C and catenary action starts at around 500 °C. The maximum ratio of the plastic strain to the elastic strain, $q_{(i)}$, at a certain temperature, $T_{(i)}$ is derived from the FE results of the parametric study. Note that $q_{(i)}$ can be written using the equation below:

$$q_i = \begin{cases} 50 \times \sqrt{\frac{30}{500-T_i}} & \text{for } T_{P_{max}} < T_i < 470^\circ\text{C} \\ 50 & \text{for } T_i > 470^\circ\text{C} \end{cases} \quad (21)$$

where $T_{P_{max}}$ is the temperature that causes lower beam flange buckling.

After plastic buckling of the lower beam flange occurs, the tangent modulus of elasticity of the beam, $E_{Tb(i)}$, is used. The axial force at any given temperature $T_{(i)}$ can be expressed as the summation of the axial force at the previous step, $P_{(i-1)}$, and the axial force increment caused by the temperature increment ΔT . The axial force can be written as:

$$P_{(i)} = P_{(i-1)} + E_{Tb(i)} A_{bc(max)} \alpha_{(i)} \Delta T \frac{k_{(i)}}{\left(\frac{E_{Tb(i)} A_{bc(max)}}{L_b} + k_{(i)}\right)} q_{(i)} \quad (22)$$

At this stage, the plastic buckling of the beam as well as the yielding of the column web and flange near the contact region causes a significant increase in the beam deflection. The significant deflection in the beam at about 500 °C causes the whole beam section to act in catenary. However, due to previous buckling in the beam section, the buckled area is not taken into account. The area of the beam section working in catenary, A_{ct} , becomes:

$$A_{ct} = A_b - A_{bc(max)} \quad (23)$$

The axial force in the beam can be written as follows:

$$P_{(i)} = P_{(i-1)} + E_{Tb(i)} A_{ct} \alpha_{(i)} \Delta T \frac{k_{(i)}}{\left(\frac{E_{Tb(i)} A_{ct}}{L_b} + k_{(i)}\right)} q_{(i)} \quad (24)$$

The significant geometric deformation in the beam and connection causes tensile and bending forces to develop in the tension bolts and might lead to bolt failure. The bolt force needs to be checked at each temperature increment. It is assumed that the applied bolt force is increased by a factor of 15% to account for bending due to large deformation of the connection.

At any given temperature, $T_{(i)}$, the bolt force is given by the following equation:

$$B_{f(i)} = \frac{1.15(P_{max} - P_{(i)})}{n_{tb}} \quad (25)$$

where n_{tb} is the number of tension bolts in the connection.

The critical bolt force is given as:

$$B_{cr(i)} = f_{ub(i)} A_{tb} \quad (26)$$

where A_{tb} is the area of the bolt, and $f_{ub(i)}$ is the ultimate stress in the bolt at a given temperature $T_{(i)}$. The connection fails when the bolt force $B_{f(i)}$ defined in Eq. (25) reaches the critical bolt force $B_{cr(i)}$ defined in Eq. (26).

4.4. Formulation of the response for proposed model II

4.4.1. Mechanism in (s1)

The axial force in the beam for type II mechanism in the first stage of the heating phase (s1) can be computed using Eq. (4).

As the temperature increases, the axial force developed in the beam increases and three limit states might occur: (1) column web buckling, (2) local elastic beam web buckling, and (3) beam web yielding. The force that causes buckling in the column is given in Eq. (5).

The load ratio in mechanism type II is large (>0.85). The beam develops large stresses prior to heating. These stresses lead to a reduction in the critical beam web buckling load $P_{crbw(i)}$ accounted for in Eq. (7). It is assumed that 25% of the applied moment is transferred from the beam to the connection. The critical beam web buckling load, $P_{crbw(i)}$, can be written as follows:

$$P_{crbw(i)} = \frac{\pi^2 E_{b(i)} I_b}{L_b^2} \left(\frac{A_{bw}}{A_b}\right)^2 - \frac{0.25M}{d_p} \quad (27)$$

where d_p corresponds to the depth of the endplate, and M corresponds to the applied moment on the beam at ambient temperature.

The load that causes yielding of the beam web can be written as follows:

$$P_{bwy(i)} = f_{by(i)} A_{tbp} - \frac{0.25M}{d_p} \quad (28)$$

where $f_{by(i)}$ corresponds to the yield stress in the beam, A_{tbp} corresponds to the tributary area of the beam web in the vicinity of the plate. (Fig. 10(c)).

For each temperature increment, the axial force $P_{(i)}$ (Eq. (4)) is compared to the limit states loads (Eq. (5)), Eq. (27), and Eq. (28)). The incremental procedure continues until any of the limit states is reached. Although the three limit states are checked, local buckling in the beam web occurs followed by beam web yielding.

4.4.2. Mechanism in (s2)

When local buckling of the beam web occurs, the area of the beam contribution to the axial force is reduced (similar to mechanism type I). The reduced area of the beam web is determined using Eq. (11). The values of a_1 and b_1 can be found in Table 2.

The total axial force in the beam is given by Eq. (12). The reduction in the area of the beam web continues until yielding of the beam web occurs. This occurs when the axial force, $P_{(i)}$, given by Eq. (12) reaches the beam web yielding load, $P_{bwy(i)}$, given by Eq. (28).

4.4.3. Mechanism in (s3)

After the onset of yielding of the beam web occurs, the axial force, P_i , can be written as follows:

$$P_{(i)} = P_{(i-1)} + \frac{k_{(i)} E_{Tb(i)} A_{bwr} \alpha_{(i)} \Delta T}{\left(\frac{E_{Tb(i)} A_{bwr}}{L_b} + k_{(i)}\right)} \quad (29)$$

where A_{bwr} is the minimum reduced area obtained in (s2).

The incremental procedure continues until contact occurs between the lower beam flange and the column, when the beam end rotation reaches the geometric contact angle given in Eq. (13).

The beam end rotation for a simply supported beam in the plastic range is given by Selamat and Garlock [16]:

$$\theta_{(i)} = \frac{w L_b^3 P_{(i)}}{24 E_{b(i)} I_b} \quad (30)$$

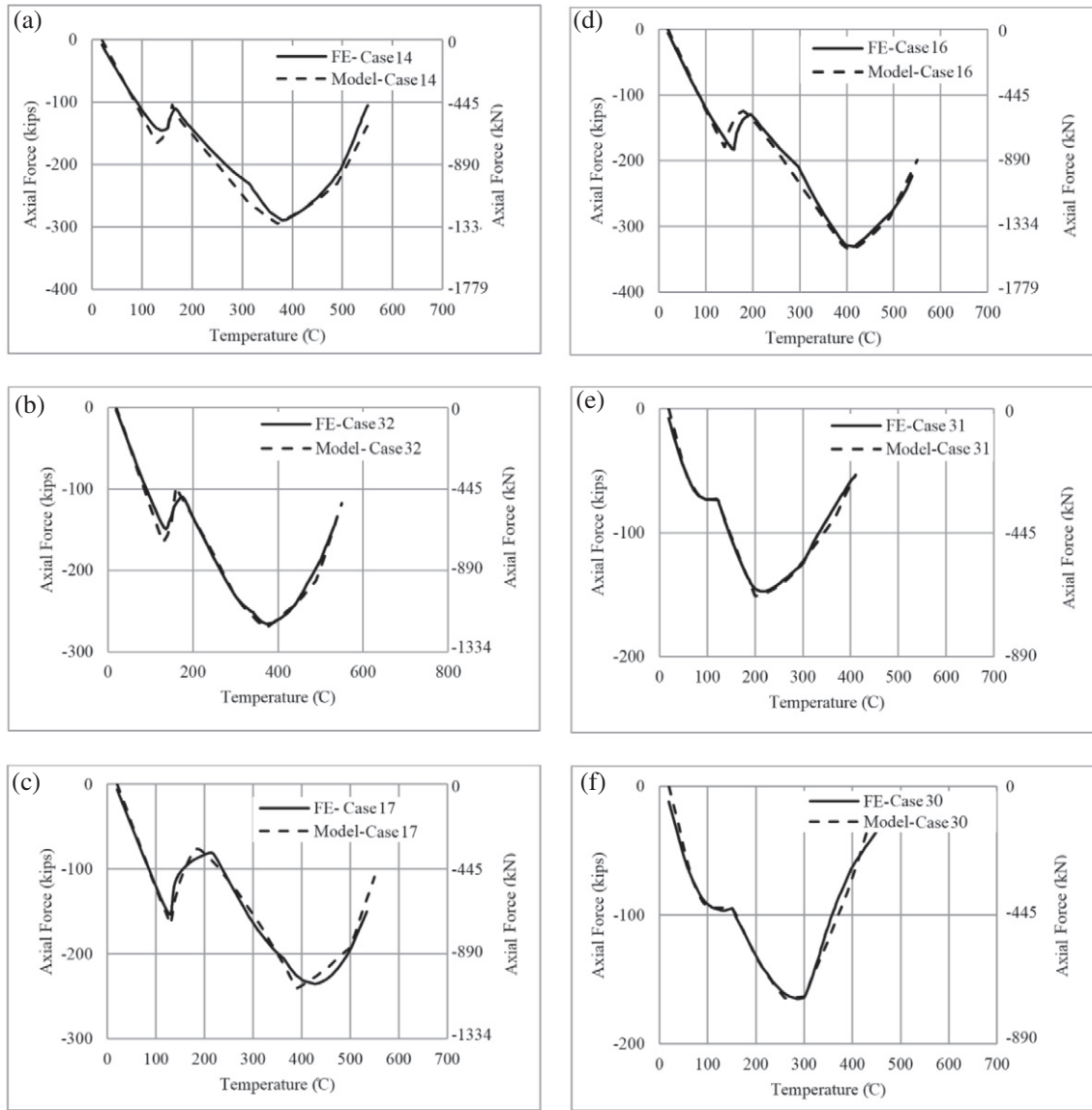


Fig. 12. FE vs. proposed model for different cases: (a) case 14, (b) case 32, (c) case 17, (d) case 16, (e) case 31, (f) case 30.

4.4.4. Mechanism in (s4)

When contact occurs, the lower beam flange becomes in a compression phase. Note that the lower beam flange contact area is in the elastic state while the beam web area is in the plastic state. The flange contact area is calculated as per Eq. (17) where a_2 and b_2 can be found in.

Table 2. The internal axial force in the beam can be written as follows:

$$P_{(i)} = k_{(i)}\Delta = \frac{k_{(i)}E_{Tb(i)}A_{bwr}\alpha_{(i)}\Delta T}{\left(\frac{E_{Tb(i)}A_{bwr}}{L_b} + k_{(i)}\right)} + \frac{k_{(i)}E_{b(i)}A_{bfc(i)}\alpha_{(i)}\Delta T}{\left(\frac{E_{b(i)}A_{bfc(i)}}{L_b} + k_{(i)}\right)} \quad (31)$$

The axial compressive force is limited by local lower flange buckling followed by yielding of the lower flange.

The load that causes local buckling in the lower flange of the beam is given by the following formula:

$$P_{crbf(i)} = \frac{\pi^2 E_{b(i)} I_b}{L_b^2} \left(\frac{A_{bfc(i)}}{A_b}\right)^2 - \frac{0.25M}{d_p + I_1} \quad (32)$$

4.4.5. Mechanism in (s5)

After local buckling occurs in the lower beam flange, the flange contact area is reduced. The axial force in the beam can be written as follows:

$$P_{(i)} = k_{(i)}\Delta = \frac{k_{(i)}E_{T(i)}A_{bwr}\alpha_{(i)}\Delta T}{\left(\frac{E_{T(i)}A_{bwr}}{L_b} + k_{(i)}\right)} + \frac{k_{(i)}E_{b(i)}A_{bfr(i)}\alpha_{(i)}\Delta T}{\left(\frac{E_{b(i)}A_{bfr(i)}}{L_b} + k_{(i)}\right)} \quad (33)$$

where $A_{bfr(i)}$ corresponds to the reduced lower beam flange contact area (current step).

The incremental procedure continues until lower beam flange yielding occurs. The load that causes lower beam flange yielding is given by the following equation:

$$P_{bfy(i)} = f_{by(i)}A_{bfr(i)} - \frac{0.25M}{d_p + I} \quad (34)$$

4.4.6. Mechanism in (s6)

After buckling of the lower beam flange occurs, followed by lower beam flange yielding, the axial force can be computed as per Eq. (22) and Eq. (24) (depending if temperature below or above 500 °C, respectively). The bolts fail when the bolt force reaches the critical bolt force.

5. Mechanistic model vs. FE results

The stiffness terms are derived to be applied in an incremental computer automated iterative solution as shown in Fig. 11. The two proposed models and the possible limit states are summarized in the flowchart (Fig. 11). Figs. 12 and 13 show a comparison of the mechanistic model with the FE results for different cases (14, 32, 17, 16, 31 and 30) (Table 2). It can be seen that the proposed model predicts the axial force in the beam with excellent agreement for all the cases. It also predicts tension bolt failure which occurs in the heating stage of the fire.

6. Conclusions

Key results of a computational study on the behavior of shear endplate connections in fire were presented in this paper. FE models of shear endplate connections were developed and validated against data from elevated temperature tests conducted at the University of Sheffield [18]. FE models for connection assemblies were then used to investigate the effect of key geometric and material parameters on the behavior of shear endplate connections during a fire. A mechanistic model that predicts the force-temperature response and quantifies the thermal-induced axial forces and deformations was developed for the connection assembly. The following conclusions are made from this research:

- FE models predict with reasonable accuracy the total force-rotation response, capacity, and failure mode (plate rupture at the toe of the weld) of the shear endplate connection at ambient and elevated temperature.
- Parametric studies were conducted on a beam connected at each end to columns using shear endplate connections. Very large compressive axial forces develop during the heating stage of a fire at about 300 °C to 400 °C. Shear endplate connections are therefore vulnerable to failure during the heating stage of a fire.
- The results of these simulations suggest that very large axial compressive forces would be expected at beam end connections for structures that have been provided insulation in accordance with U.S. building standards. That is, structures in full compliance with U.S. standards for structural-fire resistance may be vulnerable to failure at beam end connections. Note that current U.S. building standards for structural fire resistance do not explicitly consider beam-to-column connections.
- The shear endplate connections evaluated in this parametric study were only designed for gravity loads, as is typical in design practice. That is, the large axial forces expected at the connections during a fire event were not considered in the connection design. The simulations suggest that most of the connections considered in these parametric studies would likely fail in the heating stage of a fire. The governing failure mode is tension bolt failure.
- The parametric study performed on shear endplate connections shows that among the factors evaluated in this study, the main ones that impact the axial force demand on the shear endplate connection are: load ratio, beam length, and endplate thickness.
- Based on the results of the FE simulations and experimental results, a mechanistic model was developed for the connection. The characteristics of the proposed model such as stiffness, tension and compression forces are determined based on each component of the connection. The model was capable of predicting the thermal induced forces in the beam and connection as well as the deformation and failure modes. The FE results were compared to the results of the proposed model, and the results were in excellent agreement. Note that the beam flange and web slenderness were not included in the formulation of the proposed model.

- In the proposed model, two types of mechanisms are modeled based on the FE results of the parametric study: mechanism type I (load ratio < 0.85), and mechanism type II (load ratio > 0.85). The limit states encountered in the connection for the mechanism type I are (1) beam web buckling, (2) lower flange buckling, (3) tension bolt failure (failure mode). The limit states encountered in the connection for mechanism type II are (1) local beam web buckling, (2) beam web yielding, (3) local lower flange buckling, (4) lower flange yielding, (5) tension bolt failure (failure).
- One of the main advantages of the proposed mechanistic model is that, in addition to its accuracy, it requires much less computational effort than that required using FE analysis, and can be used as well in more advanced modeling applications for fire design.

Acknowledgments

The authors gratefully acknowledge the financial support provided by the American University of Beirut Research Board under grant no. 103187-23310, and by the Lebanese National Council for Scientific Research (LNCRSR) under grant no. 103091-22968.

References

- [1] N. Ramli-Sulong, A. Elghazouli, B. Izzuddin, Behaviour and design of beam-to-column connections under fire conditions, *Fire Saf. J.* 42 (6–7) (2007) 437–451.
- [2] C. Bailey, I. Burgess, R. Plank, Analyses of the effects of cooling and fire spread on steel-framed buildings, *Fire Saf. J.* 26 (4) (1996) 273–293.
- [3] K. Al-Jabri, The Behavior of Steel and Composite Beam-to-column Connections in Fire PhD dissertation University of Sheffield, 1991.
- [4] K. Al-Jabri, Component-based model of the behavior of flexible end-plate connections at elevated temperatures, *Compos. Struct.* 66 (1–4) (2004) 215–221.
- [5] K. Al-Jabri, I. Burgess, R. Plank, Moment-rotation-temperature curves for semi-rigid joints, *J. Constr. Steel Res.* 61 (3) (2005) 281–303.
- [6] K. Al-Jabri, I. Burgess, R. Plank, Spring-stiffness model for flexible end-plate bare-steel joints in fire, *J. Constr. Steel Res.* 61 (12) (2005) 1672–1691.
- [7] Y. Hu, B. Davidson, I. Burgess, R. Plank, Experimental study on flexible end plate connections in fire, Eurosteel, 5th European Conference on Steel and Composite Structures, 2008 (3–5 September, Graz, Austria).
- [8] H. Yu, I. Burgess, J. Davison, R. Plank, Component modelling of flexible end-plate connections in fire, *Steel Struct.* 9 (1) (2009) 1–15.
- [9] W. Wang, G. Li, Y. Dong, Experimental study and spring-component modelling of extended end-plate joints in fire, *J. Constr. Steel Res.* 63 (8) (2007) 1127–1137.
- [10] W. Wang, G. Li, Y. Dong, A practical approach for fire resistance design of extended end-plate joints, *J. Constr. Steel Res.* 64 (12) (2008) 1456–1462.
- [11] G. Hu, M. Engelhardt, Studies on the behavior of steel single-plate beam end connections in a fire, *Struct. Eng. Int.* 22 (4) (2012) 462–469.
- [12] G. Hu, M. Engelhardt, Experimental investigation of steel single plate beam end connections at elevated temperature, *Eng. Struct.* 58 (2014) 141–151.
- [13] A. Daryan, M. Yahyai, Modeling of bolted angle connections in fire, *Fire Saf. J.* 44 (7) (2009) 976–988.
- [14] V. Kodur, M. Naser, P. Pakala, A. Varma, Modeling the response of composite beam-slab assemblies exposed to fire, *J. Constr. Steel Res.* 80 (2013) 163–173.
- [15] S. Selamet, M. Garlock, A comparison between the single plate and angle shear connection performance in fire, *ASCE Structures Congress 2011*, pp. NV:416–NV:426 Las Vegas.
- [16] S. Selamet, M. Garlock, Predicting the maximum compressive beam axial force during fire considering local buckling, *J. Constr. Steel Res.* 71 (2012) 189–201.
- [17] S. Selamet, M. Garlock, Fire resistance of steel shear connections, *Fire Saf. J.* 68 (2014) 52–60.
- [18] University of Sheffield, EPSRC project EP/C510984/1: Robustness of Joints in Fire, <http://fireresearch.group.shef.ac.uk/downloads.html> 2008 (February 2014).
- [19] R.I. Dassault Systems, K. Hibbitt, Sorensen, ABAQUS Version 6.12 User's Manual, 2012.
- [20] American Institute of Steel Construction (AISC), Specification for Structural Steel Buildings ANSI/AISC 360-10 2010 (Chicago, IL).
- [21] J. Lee, M. Morovat, G. Hu, M. Engelhardt, E. Taleff, Experimental investigation of mechanical properties of ASTM A992 steel at elevated temperatures, *Eng. J.* 50 (4) (2013) 249–272.
- [22] American Institute of Steel Construction (AISC), Specification for Structural Steel Buildings ANSI/AISC 360-10 2015 (Chicago, IL).
- [23] European Committee for Standardization (CEN), Eurocode 3: Design of Steel Structures - Part 1-8: Design of Joints and Building Frames, 2005 (BS EN 1993-1-8, Brussels).
- [24] E. Hantouche, S. Sleiman, Response of double angle and shear endplate connections at elevated temperatures, *Int. J. Steel Struct.* 16 (2) (2016) 489–504.
- [25] T. Li, D. Nethercot, B. Choo, Behaviour of flush end-plate composite connections with unbalanced moment and variable shear/moment ratios II. Prediction of moment capacity, *J. Constr. Steel Res.* 38 (2) (1996) 165–198.
- [26] A. Usmani, J. Rotter, S. Lamont, A. Sanad, M. Gillie, Fundamental principles of structural behavior under thermal effects, *Fire Saf. J.* 36 (2001) 721–744.